Molecular Neurobiology (2019) 56:3722–3735
https://doi.org/10.1007/s12035-018-1335-y

Ablation of Cytochrome *c* in Adult Forebrain Neurons Impairs Oxidative Phosphorylation Without Detectable Apoptosis

Milena Pinto[1] · Uma D. Vempati[1,2] · Francisca Diaz[1] · Susana Peralta[1] · Carlos T. Moraes[1,2]

Received: 14 June 2018 / Accepted: 27 August 2018 / Published online: 6 September 2018

Abstract

Cytochrome *c* (Cyt *c*), a heme-containing mitochondrial protein, has a critical function in both respiration and apoptosis. Consistent with these vital functions, somatic Cyt *c* mouse knockout is embryonic lethal. In order to investigate the sensitivity of postnatal neurons to Cyt *c* depletion, we developed a neuron-specific conditional knockout model. Neuron-specific Cyt *c* KO mouse ($nCytc^{KO}$) was created by crossing the floxed Cyt *c* mouse with a CamKIIα-cre transgenic mouse, which deletes the floxed alleles postnatally. $nCytc^{KO}$ mice were normal at birth but developed an abnormal phenotype starting at 8 weeks of age with weight loss, tremor, decreased sensorimotor coordination, and sudden death between 12 and 16 weeks. Histological analysis did not show major neuronal degeneration. Analyses of oxidative phosphorylation showed a specific reduction in complex IV levels. Markers of oxidative stress were also increased. This novel model showed that neuronal complex IV is destabilized in the absence of Cyt *c*. It also showed that ablation of Cyt *c* in neurons leads to severe behavioral abnormalities and premature death without detectable neuronal loss, suggesting that neurons have the potential to survive for extended periods of time without a functional OXPHOS.

Keywords Cytochrome *c* · Mitochondrial dysfunction · Conditional knock out

Abbreviations

3-MT	3-Methoxytyramine/3-methoxy-4-hydroxyphenethylamine
Apaf1	Apoptotic protease activating factor 1
BAD	Bcl-2-associated death promoter
BAX	Bcl-2-associated X protein
Bcl2	B cell lymphoma 2
BN-PAGE	Blue native polyacrylamide gel electrophoresis
CamKIIα	Calcium/calmodulin-dependent protein kinase II-α
Cyt *c*	Cytochrome *c*
$Cytc^{TG}$	Transgene
$Cytc^{HET}$	Heterozygous
$nCytc^{KO}$	Neuronal KO
COX	Cytochrome *c* oxidase, complex IV
DAPI	4′,6-Diamidino-2-phenylindole
DOPAC	3,4-Dihydroxyphenylacetic acid
ETC	Electron transport chain
GFAP	Glial fibrillary acidic protein
GPX1	Glutathione peroxidase 1

Electronic supplementary material The online version of this article (https://doi.org/10.1007/s12035-018-1335-y) contains supplementary material, which is available to authorized users.

✉ Milena Pinto
mpinto@med.miami.edu

✉ Carlos T. Moraes
cmoraes@med.miami.edu

Uma D. Vempati
uvempat@gmail.com

Francisca Diaz
FDiaz1@med.miami.edu

Susana Peralta
susanaperalta76@gmail.com

[1] Department of Neurology, Miller School of Medicine Miami, University of Miami, 1420 NW 9th Avenue, TSL Building, Rm. 231, Miami, FL 33136, USA

[2] Neuroscience Program, Miller School of Medicine Miami, University of Miami, 1420 NW 9th Avenue, TSL Building, Rm. 231, Miami, FL 33136, USA

H&E	Hematoxylin-eosin
HVA	Homovanillic acid
mtDNA	Mitochondrial DNA
NADH	Nicotinamide adenine dinucleotide
NDUFB8	NADH dehydrogenase [ubiquinone] 1 beta subcomplex subunit 8
OXPHOS	Oxidative phosphorylation
ROS	Reactive oxygen species
SDHA	Succinate dehydrogenase complex, subunit A
SOD1, SOD2	Superoxide dismutase 1/2
TUJ1	Neuron-specific Class III β-tubulin
TUNEL	Terminal deoxynucleotidyl transferase dUTP nick end labeling
UQCRFS1	Ubiquinol-cytochrome *c* reductase, Rieske iron-sulfur polypeptide 1
VDAC1	Voltage-dependent anion channels

Background

Mitochondria produce the majority of the cellular ATP through the oxidative phosphorylation (OXPHOS) system. OXPHOS is composed by the electron transport chain (ETC) and the ATP synthase. The mitochondrial ETC is responsible for the creation of an electron gradient through the mitochondrial inner membrane and consists of four multisubunit complexes: complex I (NADH-ubiquinone oxidoreductase), complex II (succinate-ubiquinone oxidoreductase), complex III (ubiquinone-cytochrome *c* oxidoreductase), and complex IV (cytochrome *c* oxidase, COX). ETC also contains two small electron carriers, coenzyme Q, and cytochrome *c*. The ATP synthase then uses the electrochemical gradient to synthetize ATP. Cyt *c* is a small protein, extremely conserved, that contains a heme group, shuttling electrons from complex III to complex IV. Electrons are transferred from reduced Cyt *c* sequentially to the CuA site, heme *a*, heme *a*3, and CuB binuclear center in the complex IV before being finally transferred to molecular oxygen to generate water [1].

In physiological conditions, Cyt *c* is anchored to cardiolipin in the mitochondrial inner membrane, but when an apoptotic stimulus perturbs the cell, Cyt *c* is released from the intermembrane space of mitochondria into the cytoplasm [2]. Here, Cyt *c* plays an important role in activating apoptosis: it interacts with Apaf-1 [3] recruiting and activating procaspase-9 [4, 5], generating the so-called apoptosome (cleaved caspase 9 plus Apaf-1). The apoptosome cleaves and activates caspase 3, starting the caspase cascade that leads to cell death.

In mammals, two different isoforms of Cyt *c* exist expressed in distinct tissues (somatic Cyt *cs* and testicular Cyt *ct*, 86% identical): the Cyt *cs* is expressed in all the tissues, while Cyt *ct* is expressed in post-meiotic male germ cells, including mature spermatozoa. In the mouse, Cyt *cs* and Cyt *ct* genes localize to chromosome 6 and 2 respectively [6]. Cyt *cs* gene contains two exons whereas Cyt *ct* gene contains four and both Cyt *cs* and *ct* show alternative splicing mRNA variants whose biological significance is still unclear [7, 8].

Due to its involvement in two vital cellular pathways (ETC and apoptosis), it is not surprising how animals knock out for the somatic isoform of Cyt *c* are embryonic lethal [9]. Disruption of testis isoform of Cyt *c*, instead, shows reduction in male fertility and early testicular atrophy but no other major abnormal phenotype [6]. To analyze the role of Cyt *c* in postnatal neurons, we created a knock-in mouse expressing a Cyt *c* transgene ($Cytc^{TG}$) flanked by LoxP sites [10] in a double knockout (Cyt *cs* and Cyt *ct*) genetic background. We then bred this mouse with a CamKIIα-cre recombinase mouse that deleted $Cytc^{TG}$ only in postnatal neurons.

The neuron-specific Cyt *c* KO ($nCytc^{KO}$) mice were indistinguishable from the controls at birth. At about 8 weeks of age, the mice developed an abnormal phenotype, which included loss of weight, kyphosis, loss of sensorimotor coordination, and tremor. Cerebral cortex and hippocampus from the $nCytc^{KO}$ mice displayed abnormal mitochondria with significant reduction in respiratory complex IV (cytochrome oxidase) activity. No significant neurodegeneration was detected even just before the premature death of mice. Mild and spotted gliosis was observed in the $nCytc^{KO}$ mouse brain, which was accompanied by increased oxidative stress. Here, we characterized the cellular and molecular consequences of Cyt *c* ablation in forebrain neurons.

Methods

Neuronal Cyt *c* KO Mice

We previously described the generation of a conditional $Cytc^{KO}$ mouse that lacks both the somatic and the testis isoforms of Cyt *c* [11]. Briefly, we obtained the Cyt *c* double isoform KO mouse by breeding Cyt $cs^{W/K}$ animals (harboring a heterozygous somatic Cyt *c* KO allele [Jackson laboratories: B6; 129-Cycstm1Wlm/J]) with Cyt $ct^{K/K}$ mice [6]. The embryonic lethal phenotype of Cyt $cs^{K/K}$ was rescued by introducing a ubiquitously expressed somatic Cyt *c* transgene flanked by loxP sites (Cyt c^{TG}). To generate a neuron-specific KO, Cyt $cs^{K/K}$-Cyt $ct^{K/K}$-Cyt c^{TG} mouse was crossed with a transgenic mouse expressing cre recombinase under the control of calcium-calmodulin-dependent protein kinase II-alpha promoter (CaMKIIα-$cre^{+/-}$) [12]. Been CaMKIIα also active in the testis, only CamKIIα-$cre^{+/-}$ females were used for the breeding (females Cyt $cs^{W/K}$-Cyt $ct^{K/K}$-CaMKIIα-$cre^{+/-}$ × males Cyt $cs^{K/K}$-Cyt $ct^{K/K}$-Cyt $cTG^{+/-}$). All animals used in this work had a pure C57Bl/6J background, backcrossed for 10 generations. All experiments and animal husbandry were

performed according to a protocol approved by the University of Miami Institutional Animal Care and Use Committee. Mice were housed in a virus-antigen-free facility of the University of Miami, Division of Veterinary Resources in a 12-h light/dark cycle at room temperature and fed ad libitum.

Western Blots

Mice were perfused with phosphate-buffered saline; brains were isolated and different regions were dissected and homogenized in PBS supplemented with complete protease inhibitor mixture (Roche) [13]. Protein concentrations were determined using the DC kit (Bio-Rad Laboratories). The homogenates were resolved on SDS-PAGE gels, transferred onto a polyvinylidene difluoride (PVDF) membrane, and hybridized with the antibodies raised against Cyt *c* (Abcam), Cox1 (Mitosciences), NDUFB8, SDHA, UQCRFS1/Rieske, VDAC1/Porin (Abcam); GFAP (Cell Signaling), TUJ1 (Chemicon), Bcl2, BAD, BAX (Cell Signaling); β-actin, γ-tubulin, vinculin (Sigma); SOD1, SOD2, GPX1 (Abgent).

Depending on the size of the related protein, bands were normalized for housekeeping gene (β-actin, γ-tubulin, vinculin) or for total protein loading (visualized by stain free technology, in the Chemidoc system, Biorad). As the same blots were used for hybridization of multiple antibodies, the following figures used the same loading control: hippocampus 4w (Bcl2 and TUJ1; SOD2 and GFAP), hippocampus 8w (Bcl2 and TUJ1; BAX and SOD2; BAD and GFAP), hippocampus 12w (Bcl2 and GFAP), cortex 4w (BAD, SOD2, and GFAP; Bcl2 and TUJ1), cortex 8w (BAX, SOD2, and GFAP; BAD and TUJ1; Bcl2 and GFAP), and cortex 12w (Bcl2 and GFAP).

Enzymatic Activity Assays

Homogenates from different parts of the brain were prepared in PBS containing complete protease inhibitor cocktail (Roche diagnostics) in a volume of 10× the weight by using a motor-driven pestle. Homogenates were centrifuged at 1000×*g* for 5 min and supernatants used for enzymatic assays. CIII (ubiquinol-cytochrome *c* reductase), CIV (cytochrome *c* oxidase), and CS (citrate synthase) activities were measured spectrophotometrically as described previously [14]. Protein concentrations were determined using the Bio-Rad Bradford Assay Kit. Specific activity was determined and values were represented as μmoles/min/mg protein.

BN-PAGE Gels

Individual OXPHOS complexes were visualized after blue native (BN)-PAGE as previously described [15]. The gels were blotted and probed with antibodies against different OXPHOS complexes.

Immunohistochemistry

Mice were perfused with PBS followed by 4% PFA. Brains were isolated, cut in half (coronal plane), and immersed in 30% sucrose solution for 24 h. The brains were then frozen in isopentane-liquid nitrogen, mounted with OCT, and sectioned at 20-μm thickness in a cryostat. The sections were permeabilized with Triton 0.1%, blocked with BSA 2%, and incubated with a primary antibody overnight at 4 °C. Subsequently, slides were incubated with a secondary antibody tagged with fluorescent Alexa-fluor (Invitrogen) for 2 h at room temperature and visualized by confocal microscopy. The following antibodies were used: NeuN (Chemicon), GFAP (Cell Signaling), Iba1 (Wako), cleaved caspase 3 (Cell Signaling), tyrosine hydroxylase (TH) (Sigma), and 8-hydroxyguanosine (oh^{8}G QED bioscience). *TUNEL assay* was performed on the same slices with "In Situ Cell Death Detection Kit, TMR red" from Roche following manufacturer's instructions. Briefly, slides were thawed, washed in PBS 5′, permeabilized for 20′ on ice in Triton 0.1%, and Na citrate 0.1%. Slides were then washed 3× with PBS, incubated for 1 h at 37 °C with staining solution, and washed and mounted with Vectashield mounting medium containing DAPI. For positive control, slides were pre-treated with DNAse (Promega) for 1 h at 37 °C.

Neurotransmitters Quantification

Neurotransmitters and dopamine metabolite quantification measurements were performed by the Vanderbilt University CMN/KC Neurochemistry Core Lab from freshly isolated brain regions that were harvested and quickly frozen in liquid nitrogen.

Electron Microscopy

The mice were perfused with 4% paraformaldehyde and brains were dissected out. They were then post-fixed in 2% phosphate-buffered glutaraldehyde (with 100-mM sucrose) overnight at 4 °C, followed by 2% buffered OsO_4 for 1 h at room temperature. Tissue slices were further processed for EMbed plastic (Electron Microscopy Sciences) embedding. Areas were chosen for semi-thin sectioning; the 1-nm sections were stained with toluidine blue/methylene blue/sodium borate. Thin sections (90 nm) were stained with uranyl acetate and lead citrate and examined in a Philips CM-10 electron microscope (FEI Co.). Sections were cut perpendicularly to the plane of the coverslip [16].

Motor Behavioral Tests

Motor behavior tests were previously utilized and described [13, 17].

Pole Test

Pole test is a test to measure motor coordination/nigrostriatal dysfunction: animals are hung upright on a vertical pole and are given 3 min to change orientation to descend. Animals are given three trials with an average taken of the latency to descent to the base. Failure to descend or fall from the pole was given a maximum time of 3 min.

Rota Rod Test

Rota Rod (IITC Life Sciences) is a test to measure motor coordination: animals are tested with three runs on a given day with an extra run for practice. Runs are combined to find the average latency to fall. A resting period of 60 s between each run is given. Animals are required to position limbs to stay on a rotating rod accelerating from 6–20 rpm over a 180-s time period. Mice that completed the task receive a final latency time of 180 s.

Open Field Test

Open field (Med Associates Inc.) is a sensitive method for measuring gross and fine locomotor activity. It consists of a chamber and a system of 16 infrared transmitters that record the position of the animal in the three-dimensional space. With this system, not only the horizontal movement can be recorded but also the rearing activity. For our study, the animals are placed in the chamber 30 min before the test and the locomotor activities were recorded for 15 min.

Statistical Analysis

All statistical analyses were done using Graphpad Prism. Means and SEM were calculated and one-way ANOVA repeated measures with Tukey post-test were used to assess statistical significance among groups.

Results

Generation and Characterization of Cyt *c* Neuron-Specific KO Mice

We have generated a conditional KO mouse of Cyt *c* ($Cytc^{TG}$) as previously described [11]. This mouse lacks both the somatic and testicular isoforms of Cyt *c*, but was made viable by the insertion of Cyt *c* transgene flanked by loxP recognition sites ($Cytcs^{KO/KO}$-$Cytct^{KO/KO}$-$CytcTG^{+/-}$). To specifically knock out Cyt *c* in neuronal cells, we crossed the $Cytc^{TG}$ mice with a transgenic mouse expressing cre recombinase under the control of calcium-calmodulin-dependent protein kinase II-alpha (CaMKIIα) promoter (Fig. 1a). The CamKIIα promoter is active at embryonic day e18.5 and reaches full activity by postnatal day p60 [18]. The generated conditional KO mice ($nCytc^{KO}$) were viable and phenotypically indistinguishable from control mice at birth. The evidence for deletion of Cyt *c* transgene is shown in Fig. 1b: the presence of a 350-bp band demonstrates the successful recombination of the allele in neuronal tissue. In the $nCytc^{KO}$, both intact and deleted forms were seen, as the tissues contain both neurons and glia. We measured the levels of Cyt *c* protein in cortex and hippocampus of the $nCytc^{KO}$ mice, using as controls both the mice harboring the transgene ($Cytc^{TG}$) and the ones heterozygous for Cyt *cs* ($Cytc^{HET}$) (see Fig. 1a). The level of Cyt *c* was decreased in cortex and hippocampus of $nCytc^{KO}$ animals compared to the $Cytc^{HET}$ animals starting at 8 weeks of age and decreased to approximately 25% by 12 weeks (Fig. 1c; quantifications in Fig. 5b–d). The levels of Cyt *c* in the $Cytc^{TG}$ animals were lower compared to those in the $Cytc^{HET}$ animals (Fig. 1d; quantifications in Fig. 5b–d). A Kaplan-Meier survival curve showed that 90% of $nCytc^{KO}$ mice died between 12 and 16 weeks of age (Fig. 1e). Between 12 and 14 weeks of age, $nCytc^{KO}$ animals undergo a rapid decline in their general appearance, developing kyphosis (Fig. 1f), reduced weight gain (Fig. 2a, d), and tremor (supplementary video). Apart from a decrease in weight (at 12 weeks in females Fig. 2a and starting at 6 weeks in males Fig. 2d), the behavior of the $Cytc^{TG}$ was indistinguishable from $Cytc^{HET}$ mice. The lower level of Cyt *c* in other tissues of the $Cytc^{TG}$ mice is probably responsible for the smaller body weight. Despite this difference, we found that the $Cytc^{HET}$ would be a good additional control and therefore compared $nCytc^{KO}$ animals to both $Cytc^{TG}$ and $Cytc^{HET}$ mice in all the experiments.

Impaired Motor Coordination in $nCytc^{KO}$ Mice

In order to analyze the sensorimotor coordination of $nCytc^{KO}$ mice and age-matched controls, we performed different motor tests: the pole test and the Rota Rod to measure coordination, and the open field to measure gross and fine locomotor activity. Starting at 4 weeks of age, the tests were performed once every 2 weeks.

$NCytc^{KO}$ animals could perform all the tests as well as the control animals until 8 weeks of age. At 8 weeks, female $nCytc^{KO}$ started to perform worse than the control on the pole test (Fig. 2b), while males were significantly performing worse than the controls starting at 10 weeks of age (Fig. 2e). By 12 weeks of age, both males and females could not perform the test anymore (Fig. 2b, e). Also on the Rotarod, the female $nCytc^{KO}$ showed signs of impaired motor coordination 2 weeks earlier than males (Fig. 2c) and at 12 weeks of age, both males and females could not stay on the Rod for more than 60 s (Fig. 2c, f). Gross locomotor activity did not significantly change in males (Fig. S1) and in females (Fig. S2). Females were less prone to initiate movements at 8 and 10 weeks of age compared to age-matched heterozygous

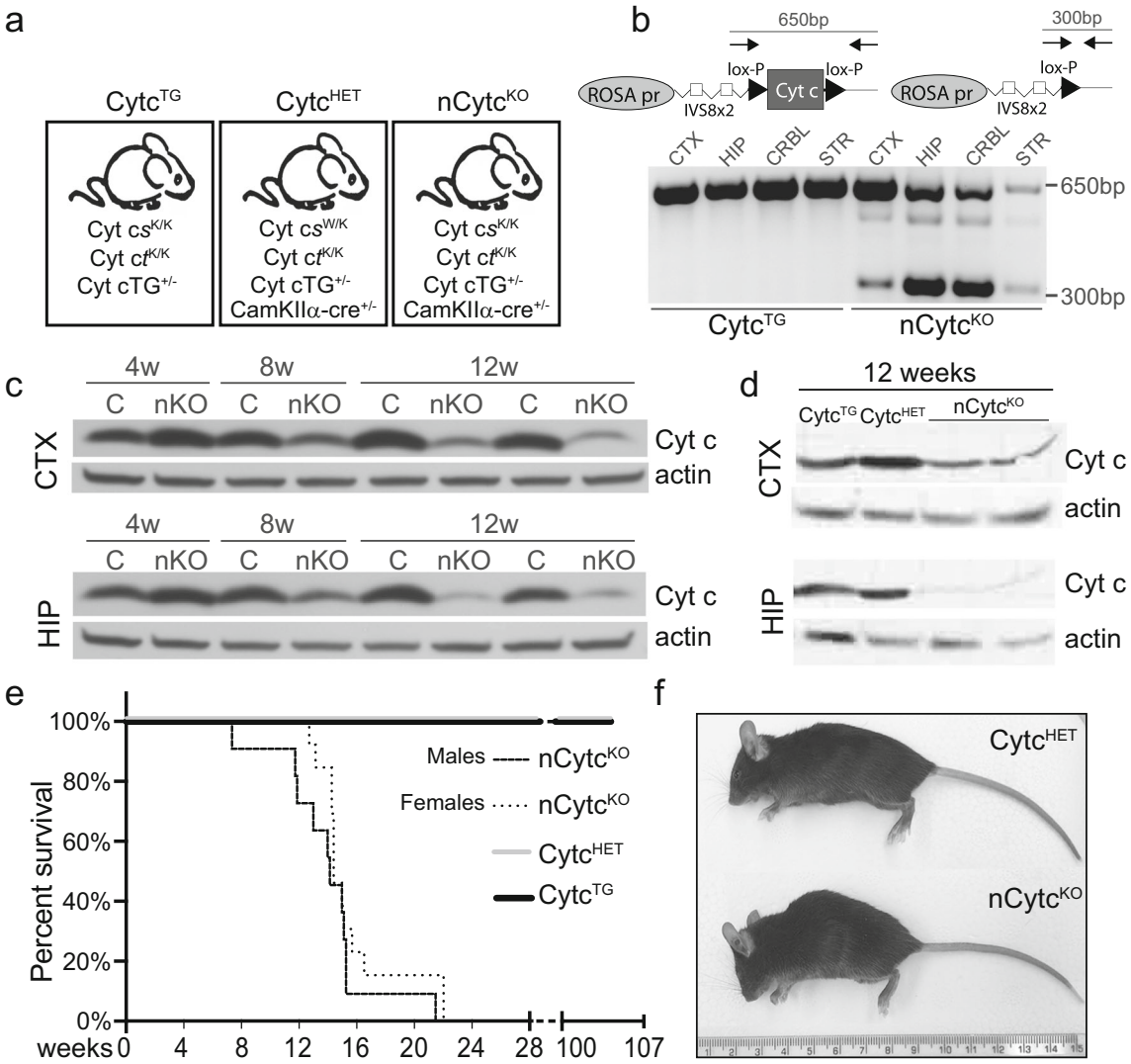

Fig. 1 Characterization of nCytc^{KO} mice. **a** Detailed description of the genetics of the mice called Cytc^{TG}, Cytc^{HET}, nCytc^{KO}. **b** Deletion of Cyt *c* transgene in the nCytc^{KO} brain tissues: schematic representation of the position of the primers on the gene, and agarose gel of the amplification. The Cyt *c* transgene was amplified: the top band is the amplification of the intact Cyt *c* TG (~ 650 bp), the bottom band is the amplification of the deleted form (~ 300 bp). **c** Representative western blot of Cyt *c* protein in wt and nCytc^{KO} mice of 4, 8, and 12 weeks of age ($n = 3$/group). Cyt *c* protein was reduced starting at 8 weeks in cortex (CTX) and hippocampus (HIP) homogenates. Actin was probed to normalize the protein loading. **d** Representative western blot of Cyt *c* protein in Cytc^{TG}, Cytc^{HET}, nCytc^{KO} of 12 weeks of age ($n = 3$/group). Cyt *c* protein was reduced also in cortex and hippocampus homogenates of Cytc^{TG} mice compared to nCytc^{HET}. Actin was probed to normalize the protein loading. **e** Survival curve shows that both females and males nCytc^{KO} mice prematurely die between 12 and 22 weeks ($p < 0.0001$), with average lifespan of 102 and 100 days, respectively. Cytc^{TG} and Cytc^{HET} do not show shorter lifespan up to 24 months ($n = 11$–15/group). **f** Representative images of 12-week-old mice showing that the nCytc^{KO} are hunched and smaller compared to Cytc^{HET}

animals (Fig. S2D). Both males and females showed less rearing activity at 12 (Fig. S1G, S1H) and 10 (Fig. S2G, S2H) weeks of age. The loss of balance/coordination was accompanied by a tremor that started at 10 weeks and was evident at 12 weeks of age in both sexes (Supplementary Video).

Motor Phenotype in nCytc^{KO} Mice Was Not Associated with Neuronal Death or Inflammation

In order to understand the basis for the phenotype, we first analyzed the gross anatomy of the brains. Brains isolated from 12-week-old nCytc^{KO} males did not show a significant difference in size (Fig. 3a) or weight (Fig. 3b), whereas brains extracted from nCytc^{KO} females were slightly but significantly smaller than those from both controls (Fig. 3c). We analyzed different brain regions of 12-week-old animals with hematoxylin eosin staining, but we did not detect any gross and massive anatomical alteration (Fig. 3d). We performed an immunohistochemical analysis with anti-NeuN as neuronal marker in 12-week-old animals' brain (Fig. 3e) and western blots with anti-TUJ1 antibody on homogenates from different brain regions (cortex, hippocampus, and striatum) of 4, 8, and

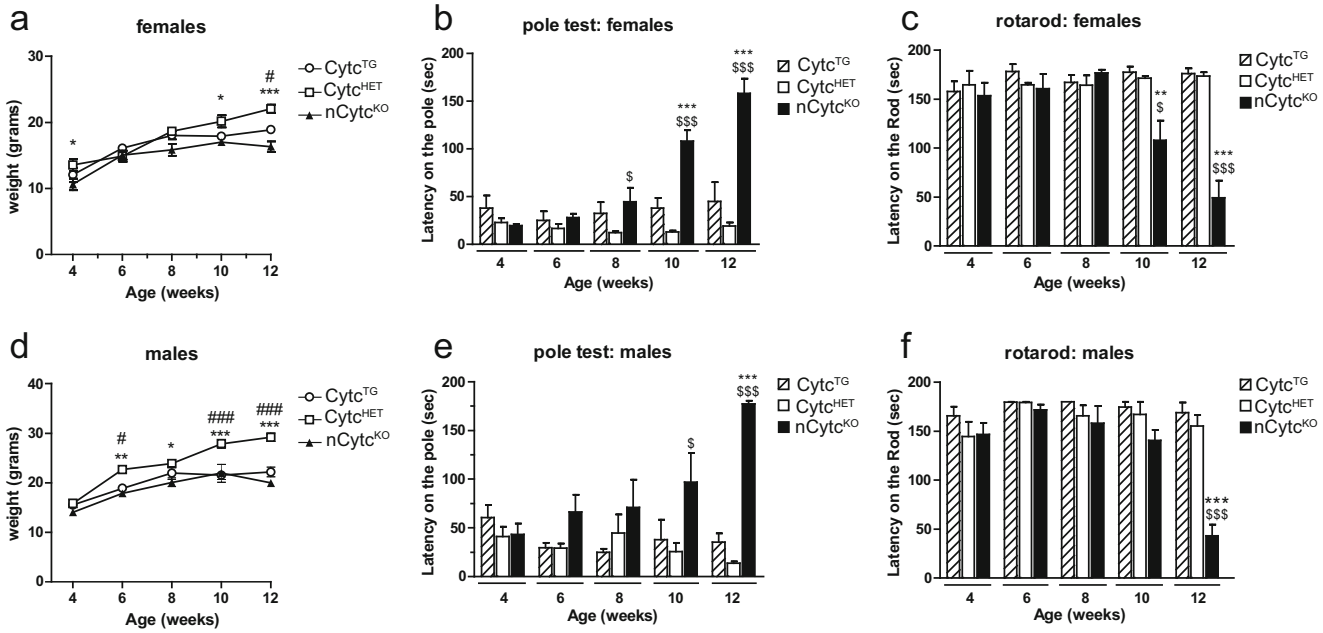

Fig. 2 Locomotive phenotypes. **a**, **d** Weight measurements (grams) of females (**a**) and males (**d**) at 4, 6, 8, 10, and 12 weeks of age ($n = 5$–10/group). **b**, **e** Pole test of females (**b**) and males (**e**) at 4, 6, 8, 10, and 12 weeks of age ($n = 14$–23/group). **c**, **f** Rotarod of females (**c**) and males (**f**) at 4, 6, 8, 10, and 12 weeks of age ($n = 7$–9/group). Error bars = SEM. *Significance between $Cytc^{HET}$ and $nCytc^{KO}$, $^{\$}$Significance between $Cytc^{TG}$ and $nCytc^{KO}$, $^{\#}$Significance between $Cytc^{TG}$ and $nCytc^{HET}$

12-week-old animals (Fig. 3f). We did not detect any gross change in the neuronal population in different areas analyzed, indicating that neuronal Cyt *c* depletion does not cause a massive neurodegeneration. All the analyses were performed on both males and females with overlapping results.

In order to understand if the motor symptoms were due to the degeneration of a particular subpopulation of neurons perhaps more sensitive to the lack of Cyt *c*, we measured neurotransmitters (Noradrenaline, Acetylcholine, GABA) in different areas of the brain, but we did not detect significant changes (Fig. S3A, S3B, S3C).

Considering that the motor symptoms in $nCytc^{KO}$ specifically affected motor coordination, we analyzed the cortical-striatum circuit, as defects in this system cause the loss of sensorimotor function in Parkinson's and Huntington's diseases [19]. Tyrosine hydroxylase (TH) is an enzyme involved in dopamine metabolism and therefore a marker of dopaminergic neurons. We examined TH^+ neurons in *substantia nigra* and locus coeruleus, and TH^+ terminals in striatum in $nCytc^{KO}$ mice (Fig. S3D) but we did not detect any changes. We also quantified dopamine, dopamine metabolites (DOPAC, HVA, 3-MT) in the striatum in $nCytc^{KO}$ mice without detecting significant changes (Fig. S3E, S3F), excluding this pathway in the etiology of the motor coordination defects and of the tremor. Alterations of Purkinje neurons in the cerebellar cortex could be the cause of the tremor and motor phenotypes [20]. However, we did not detect changes in the gross morphology of this region (Fig. S3G).

Because neurodegeneration and metabolic defects are often accompanied by neuroinflammation [21], we next examined the extent of gliosis in these animals. We performed immunohistochemistry and western blot analysis with antibodies against GFAP (marker of glial cells) and Iba1 (marker of microglia) on animals at different ages. We observed increased $GFAP^+$ cells in hippocampus and in spotted regions of motor cortex and striatum of $nCytc^{KO}$ mice compared to $Cytc^{TG}$ and $Cytc^{HET}$ (Fig. 4a, white circles). The same regions also showed increased $Iba1^+$ cells (Fig. 4b). We did not detect any significant change in the morphology of GFAP and Iba1 positive cells (Fig. 4a, b, last panel). Western blot analysis performed on cortex, hippocampus, and striatum of 1, 2, and 3-month-old animals showed a significant increase of GFAP only in hippocampus of 3-month-old $nCytc^{KO}$ (Fig. 4c, d).

Lack of Cytochrome *c* in Neurons Leads to Decreased Complex IV and Structural Mitochondrial Abnormalities

To measure the steady-state levels of respiratory complex subunits, we performed western blot analysis of cortex, hippocampus, and striatum homogenates from animals at 12 weeks of age (Fig. 5, Fig. S5). We analyzed steady-state level of NDUFB8 (CI subunit), SDHA (CII subunit), Rieske Iron-Sulfur Protein UQCRFS1 (CIII subunit), and Cox1 (CIV subunit). VDAC1 (voltage-dependent anion channel-1) is a mitochondrial outer membrane protein. As expected, Cyt *c* was decreased in the cortex (Fig. 5a, b), in the hippocampus (Fig. 5c, d), and in the striatum (Fig. S4A, 4B) of $nCytc^{KO}$ compared to $Cytc^{HET}$. We also detected a decrease in the

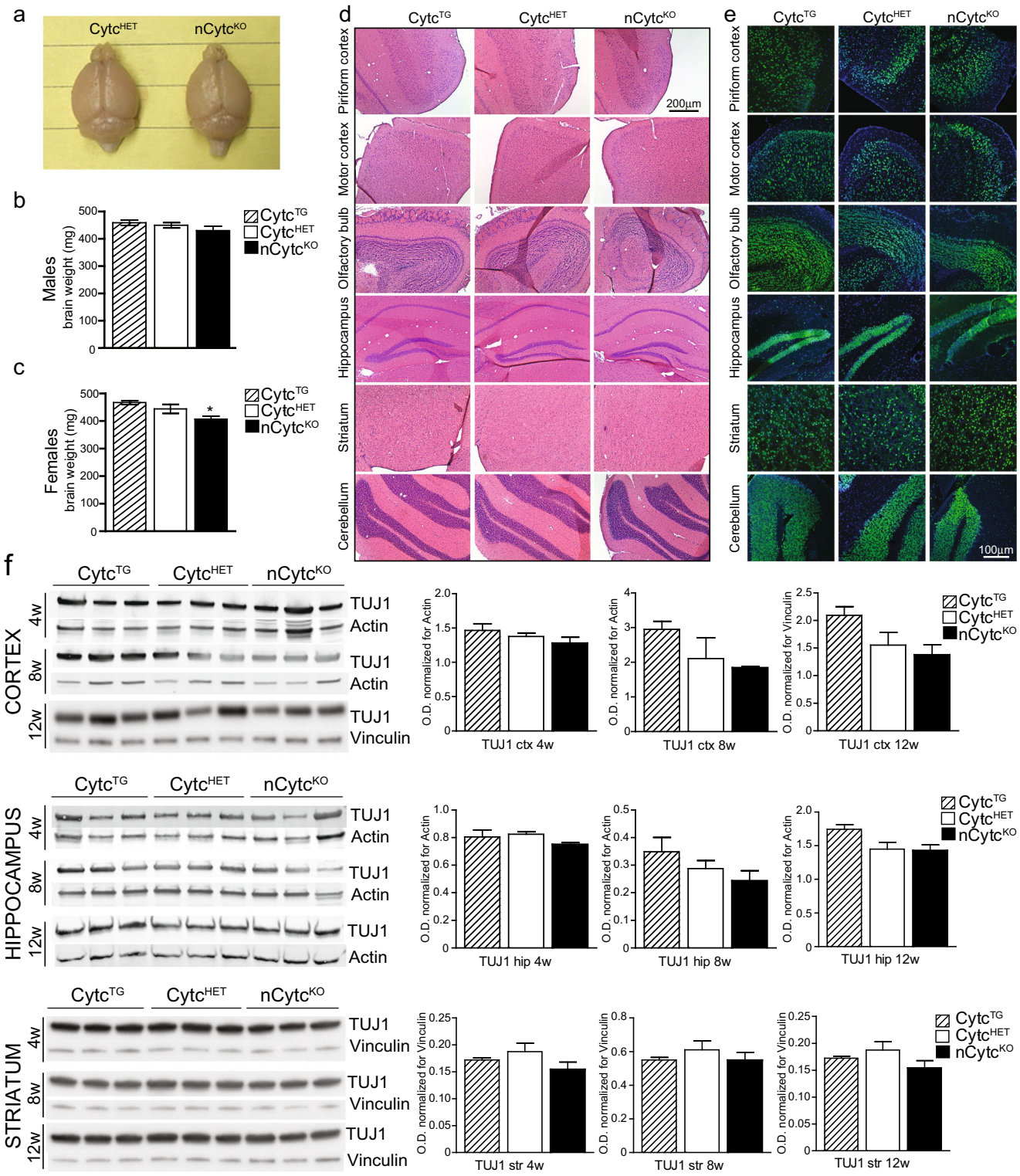

Fig. 3 Brain morphology and neurodegeneration. **a** Gross brain morphology of 12-week-old Cytc^{HET} and nCytc^{KO} mice revealed no changes. **b**–**c** Brain weight of 12-week-old Cytc^{TG}, Cytc^{HET}, and nCytc^{KO} females (**b**) and males (**c**) ($n = 6$–10/group). **d** H&E staining on different brain regions of 12-week-old animals shows no apparent difference in morphology between Cytc^{TG}, Cytc^{HET}, and nCytc^{KO}. **e** Immunohistochemical images of NeuN staining on different brain regions of 12-week-old animals show no apparent difference in cell number between Cytc^{TG}, Cytc^{HET}, and nCytc^{KO}. **f**–**g** Western blots (**f**) and relative quantifications (**g**) of protein homogenates from cortex, hippocampus, and striatum of Cytc^{TG}, Cytc^{HET}, and nCytc^{KO} at different ages (4, 8, 12 weeks) probing for neuronal marker TUJ1 show no changes in protein level. ($n = 3$/group). Error bars = SEM. *Significance between Cytc^{HET} and nCytc^{KO}

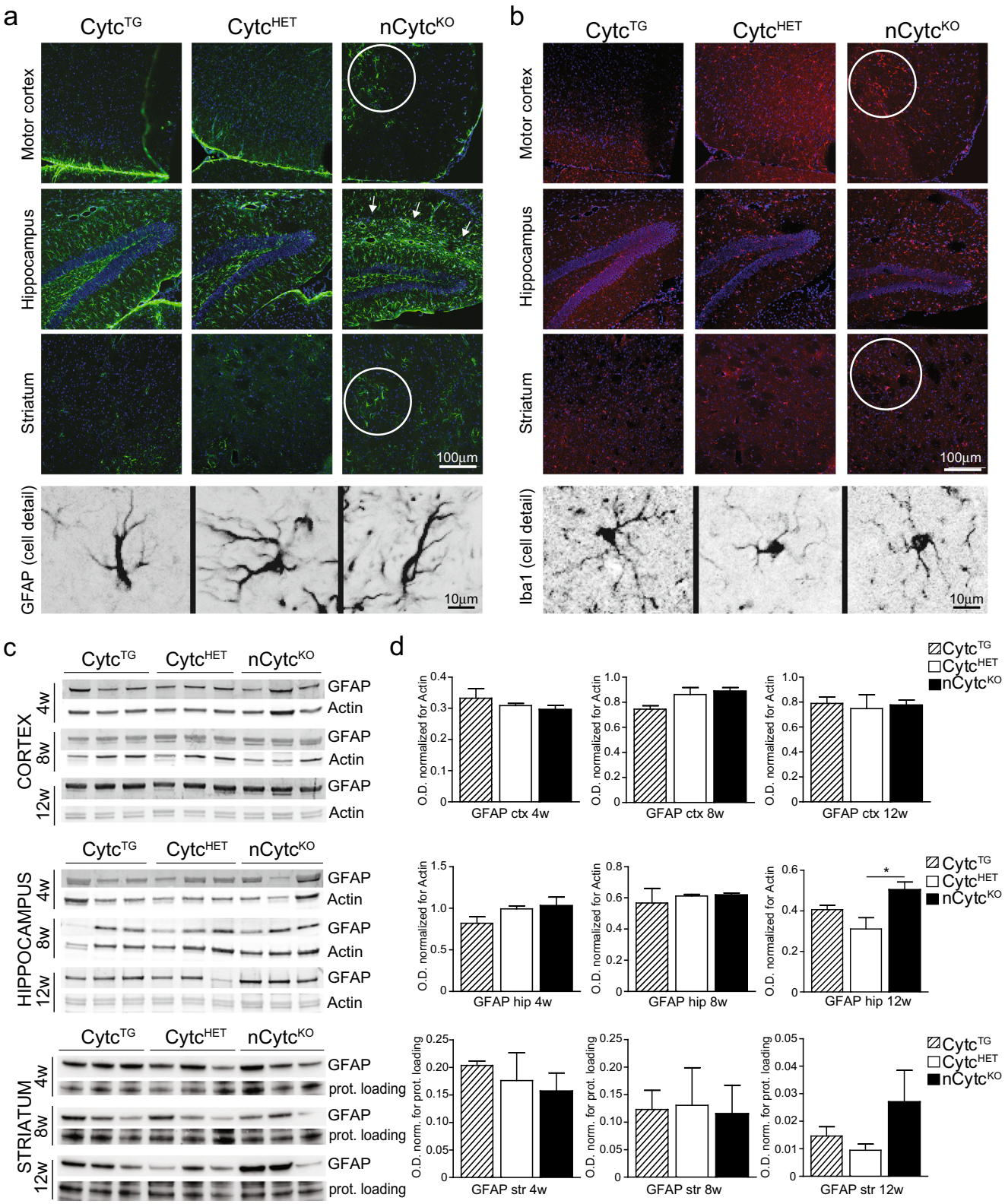

steady-state level of Cox1, a subunit of the complex IV (in the cortex Fig. 5a, b, and in the hippocampus Fig. 5c, d). The levels of NDUFB8, SDHA, and UQCRFS1 remained comparable to control values. As already mentioned, the Cytc^{TG} animals also showed a decreased level of Cyt *c*, but the levels of Cox1 were not significantly decreased.

◀ **Fig. 4** Neuroinflammation. **a–b** Immunohistochemical images of GFAP (**a**) and Iba1 (**b**) staining on different brain regions of 12-week-old animals showed increased inflammation in the hippocampi and in spotted areas (white circles) of nCytc^{KO}. The bottom panel shows representative images of GFAP+ and Iba1+ cells at higher magnification. **c–d** Western blots (**c**) and relative quantifications (**d**) of protein homogenates from cortex, hippocampus and striatum of Cytc^{TG}, Cytc^{HET}, and nCytc^{KO} at different ages (4, 8, 12 weeks) probing for glial marker GFAP. "Prot. loading" indicates that stain free technology was used for protein normalization. Increased inflammation was detected in hippocampus of 12-week-old nCytc^{KO} mice. ($n = 3$/group, error bars = SEM. *Significance between Cytc^{HET} and nCytc^{KO})

We then analyzed the steady-state levels of fully assembled oxidative phosphorylation complexes by blue native gel electrophoresis followed by western blot. Tissues were solubilized in conditions that preserve the individual mitochondrial complexes and supercomplexes. Both cortex (Fig. 5e, f) and hippocampus (Fig. 5g, h) of nCytc^{KO} showed significantly reduced levels of fully assembled complex IV. The levels of fully assembled complex I (probed with anti NDUFA9), complex II (probed with anti SDHA), complex III (probed with anti UQCRC1), and supercomplex I + III were unchanged.

We also determined the effect of the deletion of Cyt *c* on the enzymatic activity of different complexes of the electron transport chain. Deletion of Cyt *c* had an impact on CIV activity. At 12 weeks of age, nCytc^{KO} mice displayed about 60% of CIV activity compared to Cytc^{HET} in cortex (Fig. 5i) and about 51% in hippocampus (Fig. 5j). Considering that the homogenates also contain glial cells that are CamKIIα-negative cells, it is likely that the defect in affected neurons is more severe. Interestingly, also the Cytc^{TG} animals showed a reduced CIV activity compared to Cytc^{HET} mice (51% in cortex and 68% in hippocampus). Complex III and citrate synthase enzymatic activity were unchanged.

In order to analyze if the lack of Cyt *c* affects mitochondrial morphology, we also performed electron microscopy analysis of cortex and hippocampus from 3-month-old nCytc^{KO} mice. We observed a clear loss of cristae organization, in both males and females (Fig. 5k).

Deletion of Cytochrome *c* in Neurons Leads to Increased Oxidative Stress

Previous work from our lab using other models of mitochondrial dysfunctions suggested that some defects in oxidative phosphorylation in neurons can increase reactive oxygen species (ROS) damage [21]. To assess the extent of oxidative damage induced by impaired OXPHOS, we examined different brain regions of 3-month-old animals by immunohistochemistry with an antibody anti-8-hydroxyguanosine (oh^{8}G), a marker of nucleic acid oxidation. Some regions in the nCytc^{KO} showed increased staining, mainly in the hippocampus and in the striatum (Fig. 6a).

We then performed western blot analysis to measure the steady-state levels of mitochondrial superoxide dismutase 2 (SOD2) and glutathione peroxidase (GPX1), two enzymes involved in the ROS detoxification. Their increased level is considered an indirect measurement of oxidative stress, since they are overexpressed in the presence of oxidative damage. We analyzed cortex, hippocampus, and striatum homogenates from 1, 2, and 3-month-old animals and both SOD2 and GPX1 were increased in cortex and in hippocampus (Fig. 6b, c) but not in striatum (Fig. S4E, S4F) of 3-month-old nCytc^{KO}, suggesting the presence of oxidative stress.

Loss of Cytochrome *c* Is Not Associated with Increased Apoptosis

Because cortex and hippocampus of 3-month-old nCytc^{KO} showed decreased CIV activity and oxidative stress, we analyzed if the energetic imbalance and the oxidative stress induced apoptosis. Since the release of Cyt *c* from the mitochondria is one of the effector steps that will lead to the activation of the caspase cascade, we first analyzed the levels of markers that function upstream of Cyt *c* release.

One of the event that can lead to the release of Cyt *c* from the mitochondria is the oligomerization of BAX, which forms pores in the mitochondrial outer membrane. When we analyzed the levels of BAX in cortex and hippocampus of 1, 2, and 3-month-old animals, (Fig. 7a) we did not detect significant changes.

Consistent with this result, also the levels of BCL-2 (anti apoptotic protein that inhibits BAX oligomerization) and of BAD (that can activate BAX indirectly by neutralizing BCL-2) were unchanged (Fig. 7a). To further investigate if the apoptotic cascade was initiated in specific regions of the brain, we analyzed the presence of cleaved caspase 3 by performing immunohistochemistry analysis. We did not detect positive cells, neither in the motor cortex nor the hippocampus (Fig. 7b). We detected only rare neurons positive for cleaved caspase 3 in the piriform cortex of nCytc^{KO} (Fig. S5A). We obtained the same result using a TUNEL assay to detect apoptotic DNA fragmentation, only few cells were positive in the piriform cortex of nCytc^{KO} (Fig. S5B), while we did not detect positive cells in other brain regions.

Discussion

Cytochrome *c* Depletion, Neurodegeneration, and Gliosis

Mitochondrial ATP production is vital for cellular function and viability and the need for optimally functional mitochondria is particularly high for neurons due to their unique electrophysiological properties and high ATP demand [22, 23]. Impaired complex IV activity has been described in

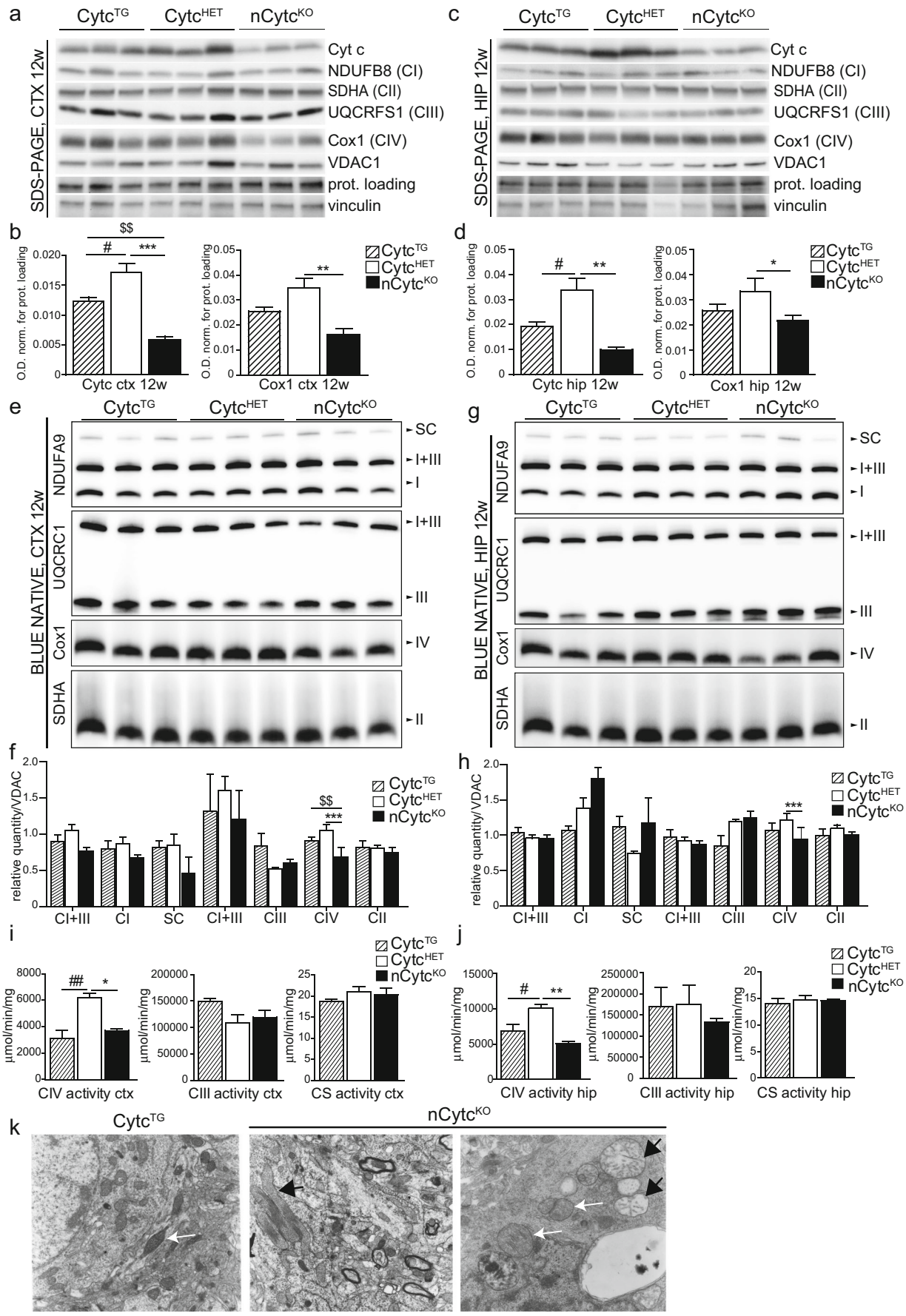
a
CytcTG
CytcHET
nCytcKO
SDS-PAGE, CTX 12w
Cyt c
NDUFB8 (CI)
SDHA (CII)
UQCRFS1 (CIII)
Cox1 (CIV)
VDAC1
prot. loading
vinculin
c
SDS-PAGE, HIP 12w
b
O.D. norm. for prot. loading
Cytc ctx 12w
Cox1 ctx 12w
d
Cytc hip 12w
Cox1 hip 12w
e
BLUE NATIVE, CTX 12w
NDUFA9
UQCRC1
Cox1
SDHA
SC
I+III
I
III
IV
II
g
BLUE NATIVE, HIP 12w
f
relative quantity/VDAC
CI+III
CI
SC
CIII
CIV
CII
h
i
µmol/min/mg
CIV activity ctx
CIII activity ctx
CS activity ctx
j
CIV activity hip
CIII activity hip
CS activity hip
k

◀ **Fig. 5** Mitochondrial proteins and complexes activity. **a** Western blots probing mitochondrial oxidative phosphorylation complex subunits in cortex homogenates from Cytc^{TG}, Cytc^{HET}, and nCytc^{KO} at 12 weeks of age and **b** quantifications for Cyt *c* and Cox1. **c** Western blots probing mitochondrial oxidative phosphorylation complex subunits in hippocampus homogenates from Cytc^{TG}, Cytc^{HET}, and nCytc^{KO} at 12 weeks of age and **d** quantifications for Cyt *c* and Cox1. ($n = 3$/group, error bars = SEM. $^{\$}$Significance between Cytc^{TG} and nCytc^{KO}, *Significance between Cytc^{HET} and nCytc^{KO}, $^{\#}$Significance between Cytc^{TG} and nCytc^{HET}). "Prot. loading" indicates that stain free technology was used for protein normalization. **e** BN-SDS-PAGE blots probing mitochondrial oxidative phosphorylation complexes and supercomplexes in cortex homogenates from Cytc^{TG}, Cytc^{HET}, and nCytc^{KO} at 12 weeks of age and **f** relative quantifications. **g** BN-SDS-PAGE blots probing mitochondrial oxidative phosphorylation complexes and supercomplexes in hippocampal homogenates from Cytc^{TG}, Cytc^{HET}, and nCytc^{KO} at 12 weeks of age and **h** relative quantifications. ($n = 3$/group, error bars = SEM. $^{\$}$Significance between Cytc^{TG} and nCytc^{KO}, *Significance between Cytc^{HET} and nCytc^{KO}). **i**–**j** Mitochondria respiratory complex activities in **i** cortical and **j** hippocampal homogenates from 3-month-old Cytc^{TG}, Cytc^{HET}, and nCytc^{KO}. Enzymatic activity of CIII and CIV and citrate synthase (CS) were measured spectrophotometrically. ($n = 3$/group, error bars = SEM. $^{\$}$Significance between Cytc^{TG} and nCytc^{KO}, *Significance between Cytc^{HET} and nCytc^{KO}). **k** Representative electron microscopy images from Cytc^{HET} and nCytc^{KO} brains showing normal mitochondria (yellow arrows) and mitochondria with disrupted cristae (red arrows)

neurodegenerative disorders; therefore, apart from the importance in caspase activation, Cyt *c* has a potential role in OXPHOS deficiency in neurodegeneration. To date, only two mutations in the CYCS gene have been described in patients suffering from thrombocytopenia [24, 25].

In an attempt to delineate the respiratory and the apoptotic functions of Cyt *c*, Hao et al. [26] developed a knocked-in mouse with a mutated Cyt *c* gene. The mutation (K72A) affected apoptosis but did not have major effect on respiration. The mutant mice were born at a lower frequency than expected, due to partial embryonic lethality, and they did not survive long after birth because of abnormal brain development (exencephaly). This demonstrated that the apoptotic function of Cyt *c* is required for normal brain development and lymphocyte homeostasis in mice.

In order to analyze the role of Cyt *c* in post mitotic neurons, we developed a model in which neuronal deletion of Cyt *c* occurred by 4–8 weeks of age. Neuronal nCytc^{KO} mice appeared healthy at birth and undistinguishable from the controls. Starting at 8–10 weeks, when Cyt *c* levels decrease, they started showing motor coordination defects, tremor, and decreased weight gain. By 12 weeks, they underwent a rapid decline in health, leading to premature death between 12 and 16 weeks of age. Synaptic pruning and interneuron migration continue postnatally and rely on mitochondrial function [27–29]. In nCytc^{KO} mice, there were no overt alterations in brain size and weight

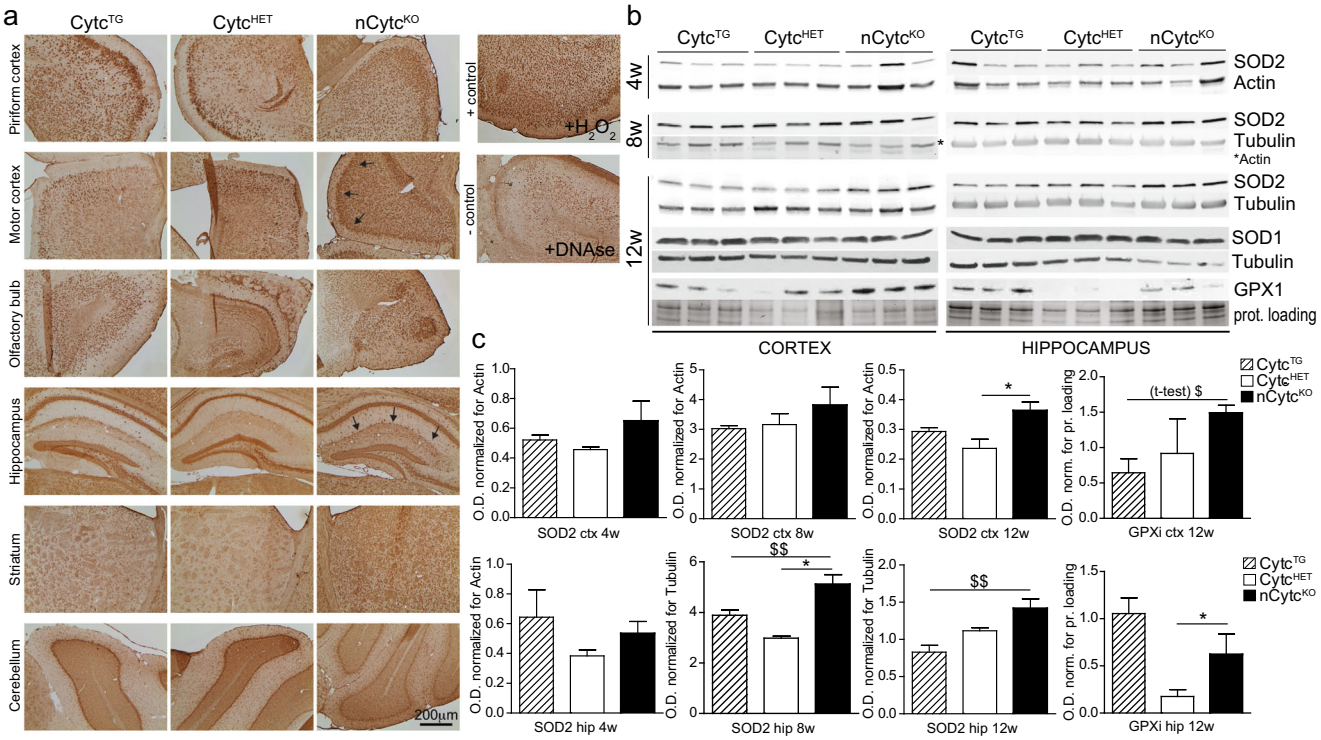

Fig. 6 Oxidative stress. **a** Immunohistochemical images of oh^{8}G staining on different brain regions of 3-month-old animals show spotted regions of oxidative damage. On the column on the right: positive (treated with hydrogen peroxide) and negative (treated with DNAse) controls. ($n = 3$/group). **b** Western blots and **c** relative quantification of SOD2 and GPX1 in protein homogenates from cortex and hippocampus of 4, 8, 12-week-old Cytc^{TG}, Cytc^{HET}, and nCytc^{KO} showed increased detoxifying enzymes in tissues from 3-month-old nCytc^{KO}. For 8-week cortex, actin (*) was used instead of tubulin as loading control. "Prot. loading" indicates that stain free technology was used for protein normalization. ($n = 3$/group, error bars = SEM. $^{\$}$Significance between Cytc^{TG} and nCytc^{KO}, *Significance between Cytc^{HET} and nCytc^{KO})

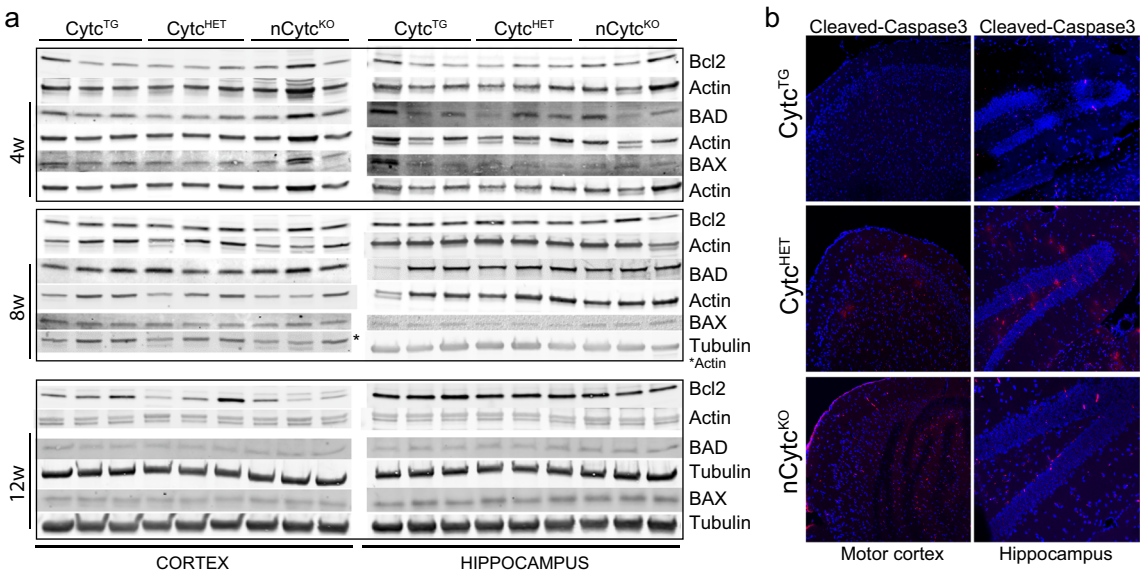

Fig. 7 Cell death. **a** Western blots with antibody anti BAD, BAX, and Bcl2. For the blot probed for Bax/8-week cortex, actin (*) was used instead of tubulin as loading control. In protein, homogenates from cortex and hippocampus of 4, 8, and 12-week-old Cytc^{TG}, Cytc^{HET}, and nCytc^{KO} showed no significant changes ($n = 3$/group). **b** Representative images of immunohistochemistry staining with antibody anti-caspase 3 (red) and DAPI (blue) on motor cortex and hippocampus of 3-month-old animals showed no areas of activated apoptosis ($n = 3$/group)

and in brain morphology, suggesting that a reduction in Cyt *c* levels during late development does not have a major impact on brain remodeling during this phase.

Several models of mitochondrial dysfunction display a phenotype where a prolonged neuronal respiratory chain deficiency is required for the induction of neurodegeneration [30, 31]. In our nCyt^{KO} model, the mitochondrial dysfunction lasted for at least 8 weeks, but we did not detect neuronal loss. We have previously demonstrated that cultured cells deficient in oxidative phosphorylation (OXPHOS) activity are protected against certain apoptotic stimuli [32]. This result was subsequently confirmed by other groups [33–35]. We also previously observed that Cyt *c* knockout cultured cell lines are resistant to both extrinsic and intrinsic apoptotic triggers [11]. The fact that we did not detect overt neurodegeneration in nCytc^{KO} mice could be explained by the resistance of the cells lacking Cyt *c* to apoptosis.

In the mitochondrial (intrinsic) pathway to cell death, the apoptotic threshold is set by interactions on the mitochondrial outer membrane between three subgroups of proteins: BH3-only proteins (BAD) which convey signals to initiate apoptosis, the pro-survival cell guardians such as BCL-2, and the pro-apoptotic effector proteins BAX [36]. These changes are upstream of the release of Cyt *c* and when we analyzed the steady-state levels of these proteins, we did not detect changes, suggesting that the apoptotic pathway was not altered. We did detect a region (the piriform cortex) in which rare neurons were positive for both cleaved caspase 3 and TUNEL assays, but it is possible that these particular neurons are not completely depleted of Cyt *c*.

It is important to note that a similar CamKIIα-deleted complex IV model (COX10 cKO) showed progressive neurodegeneration [21]. The ablation of COX10 produced a progressive complex IV deficiency, with cortex and hippocampus homogenates of COX10 cKO showing approximately 20% reduction in enzyme activity by 1 month and 70% by 4 months. At 4 months, the COX10 cKO mice showed a distinctive behavioral phenotype followed by a slower but progressive neurodegeneration; nonetheless, COX10 cKO average lifespan was around 10 months. The fact that COX10 cKO mice have even less complex IV activity compared to our nCytc^{KO} mice and they die later on [21] suggests that the premature death of the nCytC^{KO} mice is not caused simply by decreased CIV function. Because Cyt *c* is also required for respiration, it is likely that both Cyt *c* and COX10 KOs have similarly impaired OXPHOS.

It is possible that the earlier lethality observed in the nCytC^{KO} is associated with increased oxidative stress (8 weeks) and gliosis, features that were observed only at older ages in the COX10 model (by 16 weeks) [21].

Cytochrome *c* Depletion Directly Affects Complex IV Levels

In yeast, Cyt *c* is essential for the assembly of complex IV and the requirement for Cyt *c* is not related to its enzymatic activity but only to its presence in mitochondria [37]. Moreover, Cyt *c* plays not only a role in the assembly of complex IV, but it also partially protects it against proteolysis [37]. In fibroblasts lacking Cyt *c*, components of complex IV (Cox1) are decreased, as well as full-assembled complex IV and complex IV enzymatic activity [10]. Moreover, Cyt *c* depletion causes a decrease in fully assembled complex I and III and a 50% reduction in complex III enzymatic activity [10].

We show that in vivo, neuronal depletion of Cyt *c* also caused decreased levels of complex IV while steady-state levels or enzymatic activity of complex I and III was not affected.

Conclusions

In conclusion, the neuron-specific nCytC^{KO} mice developed various processes associated with neurodegeneration, namely, loss of coordination, tremor, and early death. Affected brain regions also showed oxidative stress and slightly increased gliosis but no sign of neurodegeneration or massive inflammation. These results indicate that severe neuronal phenotypes associated with OXPHOS defect are independent of neuronal death. It is likely that ATP-depleted neurons are unable to perform normal synaptic functions leading to the observed phenotypes. The blockage of the canonical apoptotic cascade may contribute to the absence of neurodegeneration.

Authors' contributions M.P. designed, performed experiments, and wrote the manuscript; U.V. designed and performed experiments and edited the manuscript; F.D. and S.P.M. performed experiments and edited the manuscript; C.T.M. designed experiments and edited manuscript. All authors read and approved the final manuscript.

Funding This work was supported by the National Institutes of Health Grants 1R01NS079965, 1R01AG036871, and 5R01EY010804 (CTM). This study was supported by the NEI center grant P30-EY014801 from the National Institutes of Health (NIH).

Compliance with Ethical Standards

All experiments and animal husbandry were performed according to a protocol approved by the University of Miami Institutional Animal Care and Use Committee.

Conflict of Interest The authors declare that they have no competing interests.

Consent to Participate Not applicable.

Consent for Publication Not applicable.

Availability of Data and Material All data generated or analyzed during this study are included in this published article [and its supplementary information files].

Competing Interests The authors declare no competing interests.

References

1. Moraes CT, Diaz F, Barrientos A (2004) Defects in the biosynthesis of mitochondrial heme c and heme a in yeast and mammals. Biochim Biophys Acta 1659(2–3):153–159
2. Kagan VE, Bayır HA, Belikova NA, Kapralov O, Tyurina YY, Tyurin VA, Jiang J, Stoyanovsky DA et al (2009) Cytochrome c/cardiolipin relations in mitochondria: a kiss of death. Free Radic Biol Med 46(11):1439–1453
3. Green DR (2005) Apoptotic pathways: ten minutes to dead. Cell 121(5):671–674
4. Li P, Nijhawan D, Budihardjo I, Srinivasula SM, Ahmad M, Alnemri ES, Wang X (1997) Cytochrome c and dATP-dependent formation of Apaf-1/caspase-9 complex initiates an apoptotic protease cascade. Cell 91(4):479–489
5. Zou H, Henzel WJ, Liu X, Lutschg A, Wang X (1997) Apaf-1, a human protein homologous to C. elegans CED-4, participates in cytochrome c-dependent activation of caspase-3. Cell 90(3):405–413
6. Narisawa S, Hecht NB, Goldberg E, Boatright KM, Reed JC, Millan JL (2002) Testis-specific cytochrome c-null mice produce functional sperm but undergo early testicular atrophy. Mol Cell Biol 22(15):5554–5562
7. Hake LE, Alcivar AA, Hecht NB (1990) Changes in mRNA length accompany translational regulation of the somatic and testis-specific cytochrome c genes during spermatogenesis in the mouse. Development 110(1):249–257
8. Hake LE, Hecht NB (1993) Utilization of an alternative transcription initiation site of somatic cytochrome c in the mouse produces a testis-specific cytochrome c mRNA. J Biol Chem 268(7):4788–4797
9. Li K, Li Y, Shelton JM, Richardson JA, Spencer E, Chen ZJ, Wang X, Williams RS (2000) Cytochrome c deficiency causes embryonic lethality and attenuates stress-induced apoptosis. Cell 101(4):389–399
10. Vempati UD, Han X, Moraes CT (2009) Lack of cytochrome c in mouse fibroblasts disrupts assembly/stability of respiratory complexes I and IV. J Biol Chem 284(7):4383–4391
11. Vempati UD, Diaz F, Barrientos A, Narisawa S, Mian AM, Millan JL, Boise LH, Moraes CT (2007) Role of cytochrome C in apoptosis: increased sensitivity to tumor necrosis factor alpha is associated with respiratory defects but not with lack of cytochrome C release. Mol Cell Biol 27(5):1771–1783
12. Dragatsis I, Zeitlin S (2000) CaMKIIalpha-Cre transgene expression and recombination patterns in the mouse brain. Genesis 26(2):133–135
13. Pickrell AM, Pinto M, Hida A, Moraes CT (2011) Striatal dysfunctions associated with mitochondrial DNA damage in dopaminergic neurons in a mouse model of Parkinson's disease. J Neurosci 31(48):17649–17658
14. Barrientos A, Fontanesi F, Diaz F (2009) Evaluation of the mitochondrial respiratory chain and oxidative phosphorylation system using polarography and spectrophotometric enzyme assays. Curr Protoc Hum Genet Chapter 19:Unit19 3
15. Diaz F, Fukui H, Garcia S, Moraes CT (2006) Cytochrome c oxidase is required for the assembly/stability of respiratory complex I in mouse fibroblasts. Mol Cell Biol 26(13):4872–4881
16. Hess RA, Miller LA, Kirby JD, Margoliash E, Goldberg E (1993) Immunoelectron microscopic localization of testicular and somatic cytochromes c in the seminiferous epithelium of the rat. Biol Reprod 48(6):1299–1308
17. Pinto M, Nissanka N, Peralta S, Brambilla R, Diaz F, Moraes CT (2016) Pioglitazone ameliorates the phenotype of a novel Parkinson's disease mouse model by reducing neuroinflammation. Mol Neurodegener 11:25
18. Xu B, Gottschalk W, Chow A, Wilson RI, Schnell E, Zang K, Wang D, Nicoll RA et al (2000) The role of brain-derived neurotrophic factor receptors in the mature hippocampus: modulation of long-term potentiation through a presynaptic mechanism involving TrkB. J Neurosci 20(18):6888–6897
19. Lanciego JL, Luquin N, Obeso JA (2012) Functional neuroanatomy of the basal ganglia. Cold Spring Harb Perspect Med 2(12):a009621
20. Miwa H (2007) Rodent models of tremor. Cerebellum 6(1):66–72
21. Diaz F, Garcia S, Padgett KR, Moraes CT (2012) A defect in the mitochondrial complex III, but not complex IV, triggers early ROS-dependent damage in defined brain regions. Hum Mol Genet 21(23):5066–5077

22. Pickrell AM, Moraes CT (2010) What role does mitochondrial stress play in neurodegenerative diseases? Methods Mol Biol 648:63–78
23. DiMauro S, Schon EA (2008) Mitochondrial disorders in the nervous system. Annu Rev Neurosci 31:91–123
24. De Rocco D et al (2014) Mutations of cytochrome c identified in patients with thrombocytopenia THC4 affect both apoptosis and cellular bioenergetics. Biochim Biophys Acta 1842(2):269–274
25. Morison IM, Cramer Bordé EM, Cheesman EJ, Cheong PL, Holyoake AJ, Fichelson S, Weeks RJ, Lo A et al (2008) A mutation of human cytochrome c enhances the intrinsic apoptotic pathway but causes only thrombocytopenia. Nat Genet 40(4):387–389
26. Hao Z, Duncan GS, Chang CC, Elia A, Fang M, Wakeham A, Okada H, Calzascia T et al (2005) Specific ablation of the apoptotic functions of cytochrome C reveals a differential requirement for cytochrome C and Apaf-1 in apoptosis. Cell 121(4):579–591
27. Bozzi Y, Casarosa S, Caleo M (2012) Epilepsy as a neurodevelopmental disorder. Front Psychiatry 3:19
28. Schafer DP, Lehrman EK, Kautzman AG, Koyama R, Mardinly AR, Yamasaki R, Ransohoff RM, Greenberg ME et al (2012) Microglia sculpt postnatal neural circuits in an activity and complement-dependent manner. Neuron 74(4):691–705
29. Lin-Hendel EG, McManus MJ, Wallace DC, Anderson SA, Golden JA (2016) Differential mitochondrial requirements for radially and non-radially migrating cortical neurons: implications for mitochondrial disorders. Cell Rep 15(2):229–237
30. Fukui H, Diaz F, Garcia S, Moraes CT (2007) Cytochrome c oxidase deficiency in neurons decreases both oxidative stress and amyloid formation in a mouse model of Alzheimer's disease. Proc Natl Acad Sci U S A 104(35):14163–14168
31. Sorensen L et al (2001) Late-onset corticohippocampal neurodepletion attributable to catastrophic failure of oxidative phosphorylation in MILON mice. J Neurosci 21(20):8082–8090
32. Dey R, Moraes CT (2000) Lack of oxidative phosphorylation and low mitochondrial membrane potential decrease susceptibility to apoptosis and do not modulate the protective effect of Bcl-x(L) in osteosarcoma cells. J Biol Chem 275(10):7087–7094
33. Park SY, Chang I, Kim JY, Kang SW, Park SH, Singh K, Lee MS (2004) Resistance of mitochondrial DNA-depleted cells against cell death: role of mitochondrial superoxide dismutase. J Biol Chem 279(9):7512–7520
34. Ludovico P, Rodrigues F, Almeida A, Silva MT, Barrientos A, Côrte-Real M (2002) Cytochrome c release and mitochondria involvement in programmed cell death induced by acetic acid in Saccharomyces cerevisiae. Mol Biol Cell 13(8):2598–2606
35. Lee MS, Kim JY, Park SY (2004) Resistance of rho(0) cells against apoptosis. Ann N Y Acad Sci 1011:146–153
36. Czabotar PE, Lessene G, Strasser A, Adams JM (2014) Control of apoptosis by the BCL-2 protein family: implications for physiology and therapy. Nat Rev Mol Cell Biol 15(1):49–63
37. Barrientos A, Pierre D, Lee J, Tzagoloff A (2003) Cytochrome oxidase assembly does not require catalytically active cytochrome C. J Biol Chem 278(11):8881–8887